Optical phonon anisotropies in the layer crystals SnS₂ and SnSe₂

G. Lucovsky and J. C. Mikkelsen, Jr.

Xerox Palo Alto Research Center, Palo Alto, California 94304

W. Y. Liang

Cavendish Laboratory, Cambridge, United Kingdom

R. M. White and R. M. Martin

Xerox Palo Alto Research Center, Palo Alto, California 94304

We have measured the far-ir reflectance spectra for the layer crystals SnS₂ and SnSe₂ for the two principal polarizations, $\vec{E} \perp \vec{c}$ and $\vec{E} \parallel \vec{c}$. We find a large difference in the frequencies of the two ir-active phonons, $\nu_{TO}(A_{2u}) > \nu_{TO}(E_u)$. Analysis of the lattice dynamics indicates that this anisotropy is due to Coulomb forces associated with charge localized on the atomic sites and as such it provides an empirical measure of the bond ionicity. On the other hand, anisotropies in the Raman modes are explained by noncentral intralayer forces, with smaller contributions from interlayer and Coulomb terms.

INTRODUCTION

This paper reports results of far-infrared reflectance measurements on the layer crystals SnS₂ and SnSe₂. There have been other studies of the ir and Raman spectra of layer crystals including MoS₂,[1] GaS and GaSe,[2] As₂S₃ and As₂Se₃,[3,4] PbI₂,[5,6] CdI₂,[6] and several of the transition-metal dichalcogenides.[7] A recurrent theme in these studies has been the very weak interlayer forces.[8] This paper treats a different aspect of layer crystals, the anisotropies in the behavior of the long-wavelength optic phonons. We compare our infrared studies with recent Raman-scattering experiments[9] and treat all of the zone-center optic modes.

SnS₂ and SnSe₂ crystals occur in the CdI₂ (or 1T) structure. The individual tightly bonded layer in SnX₂ is an X-Sn-X sandwich in which the Sn atoms are octahedrally coordinated to six nearest-neighbor X atoms. Each X atom is nested atop a triangle of Sn atoms. The three-atom basis of the unit cell gives rise to nine vibrational modes; three doubly degenerate E modes in which the atomic motions are parallel to the layer planes, and three nondegenerate A modes in which atomic motions are perpendicular to the layers. At the zone center, the irreducible representations are

$$\Gamma = A_{1g} + 2A_{2u} + E_g + 2E_u. \tag{1}$$

The acoustic modes are $A_{2u} + E_u$, so that there are four optic modes; two Raman-active modes, $A_{1g} + E_g$, and two ir-active modes, $A_{2u} + E_u$.

Layer crystals are readily grown in a platelet geometry using vapor-transport techniques. The platelet growth habit is with the c axis perpendi-

cular to the large face. This geometry allows a study of both Raman-active modes, but only one of the ir modes, the E_u mode. Recently, we have succeeded in growing large single crystals of PbI₂ and CdI₂. This enabled us to study the other ir mode, A_{2u}.[6] We found that $\nu_{TO}(A_{2u}) > \nu_{TO}(E_u)$ for both materials. We have also succeeded in growing large single crystals of SnS₂ and SnSe₂ so that both ir modes could be studied in these materials as well. We find similar anisotropies in the phonon frequencies, $\nu_{TO}(A_{2u}) - \nu_{TO}(E_u) = 135$ cm⁻¹ for SnS₂ and 97 cm⁻¹ for SnSe₂. A force-constant analysis including Coulomb terms demonstrates that these large differences in the frequencies of the ir-active modes are due almost entirely to Coulomb contributions. Anisotropies in the ir and Raman frequencies have also been explored in layer crystals having different crystal structures, MoS₂,[1] GaS and GaSe,[2] and As₂S₃.[4] The anisotropies in these crystals have been explained without the necessity to invoke Coulomb interactions. This is particularly evident in MoS₂,[1] where the ir-active modes show very weak polarization, but are separated significantly in frequency so that the large difference in frequency is clearly of a different origin than in the CdI₂-structured crystals. Conversely, it follows that a measurement of the ir-phonon frequencies in CdI₂-structured crystals then yields information regarding dipolar interactions, i.e., the local electric fields.

EXPERIMENTAL

Large single crystals of SnS₂ and SnSe₂, approximately 10 mm in diameter and 2–3 cm in length, were grown in a vertical Bridgman furnace. The crystals were not intentionally doped, but showed
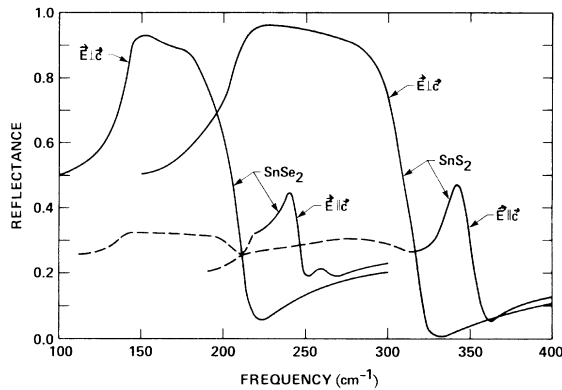
FIG. 1. Room-temperature ir-reflectance spectra of SnS_2 and $SnSe_2$. The dashed portions of the $\vec{E}||\vec{c}$ spectra indicate the extent to which surface damage mixes the $\vec{E}\perp\vec{c}$ reststrahlen band into the $\vec{E}||\vec{c}$ spectra.

weak n-type conductivities with resistivities ~1 Ω cm. ir reflectance measurements were made on freshly cleaved faces, and on faces cut and polished perpendicular to the cleavage planes. Room-temperature spectra were obtained using a PE 180 spectrophotometer. A wire-grid polarizer was used to separate spectra for $\vec{E}\perp\vec{c}$ and $\vec{E}||\vec{c}$ from the polished faces. Spectral resolution was approximately 1.5 cm^{-1} and the uncertainty in the values of the reflectance R was ~0.005.

Figure 1 displays the spectra for SnS_2 and $SnSe_2$. The spectra for $\vec{E}\perp\vec{c}$ are from the cleaved faces and those for $\vec{E}||\vec{c}$ from the polished faces. Since the polished faces require cutting and polishing perpendicular to the cleavage planes, they are less perfect than the cleaved faces. A measure of the relative surface quality was obtained from a comparison of the $\vec{E}\perp\vec{c}$ spectra from the two types of surfaces. Values of R from the polished faces were about 10% smaller than those from the cleaved faces. This reduction in R is essentially independent of frequency. Spectra for $\vec{E}||\vec{c}$ were then adjusted using this empirical surface quality factor. A second measure of the surface quality was obtained from the degree to which the $\vec{E}\perp\vec{c}$ spectrum was observed in the $\vec{E}||\vec{c}$ geometry. Both $\vec{E}||\vec{c}$ spectra show a small amount of the $\vec{E}\perp\vec{c}$ spectrum as indicated by the dashed portions of the reflectance curves in Fig. 1.

In accordance with group theory, we found one dominant reststrahl feature in each spectrum, these correspond to one transverse-optical (TO) phonon for each polarization. The reststrahlen band for $\vec{E}\perp\vec{c}$ for each crystal is stronger than the $\vec{E}||\vec{c}$ band. For example, in SnS_2 the $\vec{E}\perp\vec{c}$ band extends from ~200 to ~310 cm^{-1} with values of R within this region exceeding 0.9. In contrast, the $\vec{E}||\vec{c}$ reflectance is characterized by a narrower

feature centered at ~350 cm^{-1} with a maximum reflectance of ~0.45. Spectra for $SnSe_2$ are similar, but show weak secondary features, a broad and shallow depression at ~170 cm^{-1} in the $\vec{E}\perp\vec{c}$ spectrum and a weak subsidiary peak at ~260 cm^{-1} in the $\vec{E}||\vec{c}$ spectrum. These additional features are tentatively assigned to second-order modes and are not discussed further in this paper.

ANALYSIS

We used two techniques for analyzing the reflectance spectra: a preliminary Kramers-Kronig analysis and then an oscillator fit. This procedure was particularly useful for the $\vec{E}\perp\vec{c}$ spectra. The Kramers-Kronig analysis yielded sharp features in the dielectric functions, $\epsilon_2(\nu)$ and $-\text{Im}[1/\epsilon(\nu)]$, where $\epsilon(\nu)=\epsilon_1(\nu)+i\epsilon_2(\nu)$. The width of the peak in the energy-loss function, $-\text{Im}[1/\epsilon(\nu)]$ was greater than that of the peak in $\epsilon_2(\nu)$. For damped Lorentzian oscillators, both of these functions have the same shape and the positions of their respective peaks identify the LO and TO phonon frequencies. Two mechanisms can cause a departure from this idealized behavior. First, if second-order modes lie close to ν_{TO} or ν_{LO}, these can contribute to the linewidth or result in an asymmetric line shape, as for example in GaP.[10] A second mechanism that effects only LO modes is interaction with plasmons.[11] In particular, interaction with overdamped plasmons will broaden $-\text{Im}[1/\epsilon(\nu)]$ relative to $\epsilon_2(\nu)$.[12] We have analyzed the reflectance data with appropriate oscillator models[10,11] and have found that the second of these mechanisms is operative (see Fig. 2).

The dielectric function is then written as the sum of two frequency-dependent terms, a lattice contribution $\epsilon^{lat}(\nu)$, and a free-carrier contribution $\epsilon^{fc}(\nu)$,

$$\epsilon(\nu)=\epsilon_\infty+\epsilon^{lat}(\nu)+\epsilon^{fc}(\nu)\,, \tag{2}$$

where ϵ_∞ is the optical-frequency dielectric constant. The lattice contribution for a single-phonon mode is given by

$$\epsilon^{lat}(\nu)=S_0\nu_{TO}^2/(\nu_{TO}^2-\nu^2-i\nu\gamma_0)\,, \tag{3}$$

where S_0 is the oscillator strength and contribution of the lattice mode to the static dielectric constant, ν_{TO} is the TO phonon frequency (cm^{-1}), and γ_0 is the damping (also in cm^{-1}) The free-carrier term is given by

$$\epsilon^{fc}(\nu)=-\nu_p^2/\nu(\nu+iG_p)\,, \tag{4}$$

where ν_p^2 is a term proportional to the free-carrier density, and G_p is the damping (both are in cm^{-1}). ν_p^2 is related to the free-carrier density N by
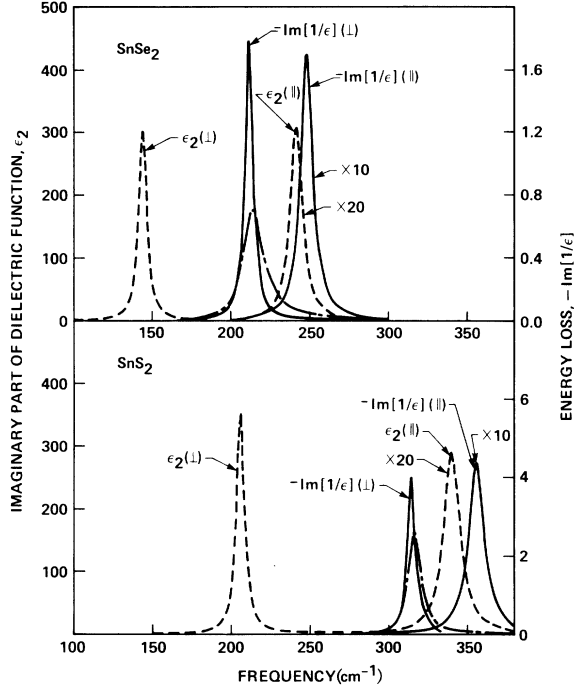
FIG. 2. Frequency dependence of the dielectric functions ϵ_2 and $-\text{Im}[1/\epsilon]$ as calculated from the oscillator parameters of Table I. The dashed-line (---) ϵ_2 functions and solid-line (——) energy-loss functions are computed using only the first-order phonon terms. The second set of energy loss curves (— - —) is calculated including the contribution of the damped plasmon as well.

$$(2\pi c)^2 \nu_p^2 = 4\pi N e^2/m^* , \tag{5}$$

where m^* is the effective mass. G_p is related to the relaxation time τ by

$$2\pi c G_p = 1/\tau . \tag{6}$$

The mobility μ is given by $\mu = e\tau/m^*$.

The plasmon mode is said to be underdamped if

$\nu_p > G_p$ and overdamped if the reverse is true, i.e., $G_p > \nu_p$. Estimates of G_p and ν_p from the dc Hall and resistivity data indicate that the plasmons in SnS_2 and $SnSe_2$ are overdamped. This means that $G_p \gg \nu$ for the frequencies of the infrared measurements. For this case

$$\epsilon^{fc}(\nu) \sim i\nu_p^2/\nu G_p \tag{7}$$

and the primary effect of the overdamped plasmon appears as a broadening of the LO phonon mode. The infrared measurements are then consistent with coupling to overdamped plasmons. In contrast, for the underdamped plasmon, two coupled LO phonon plasmon modes result.[11]

Table I contains the oscillator parameters for SnS_2 and $SnSe_2$. These were obtained through a computer-directed iterative search. The spectra for $\vec{E} \perp \vec{c}$ required both plasmon and phonon terms. The spectra for $\vec{E} \| \vec{c}$ required only phonon terms. This is simply related to the sharpness of these modes which renders them insensitive to the overdamped plasmons. For the $\vec{E} \perp \vec{c}$ bands, the reststrahl width is considerably greater than the phonon damping, for SnS_2, 109 cm^{-1} as compared to 6 cm^{-1}, so that the contribution to ϵ_2 at the leading edge of the reststrahlen band from the plasmon mode is large compared to the contribution to ϵ_2 from the lattice mode. In contrast, the width of the reststrahlen band for $\vec{E} \| \vec{c}$ is comparable to the phonon damping so that the plasmon contribution is not as important for that polarization.

Table I also contains properties of the phonon modes that are derived from the oscillator parameters. The first of these is the macroscopic transverse effective charge $e_T^*(j)$ (Ref. 13); the index j indicates the polarization, either perpendicular or parallel to c. $e_T^*(j)$ is given by

$$e_T^*(j) = 1.43 \times 10^8 \frac{(\overline{m})^{1/2}[s_0(j)]^{1/2}\nu_{TO}(j)}{N_0^{1/2}} , \tag{8}$$

TABLE I. Phonon parameters.

Material		ϵ_∞	ν_{TO} (cm^{-1})	S_0	γ (cm^{-1})	ν_{LO} (cm^{-1})	$\dfrac{e_T^*}{e}$
			Phonons			Derived parameters	
SnS_2	$\vec{E} \perp \vec{c}$	7.57	205	10.2	5.95	314	3.52
	$\vec{E} \| \vec{c}$	5.65	340	0.53	12.2	356	1.32
$SnSe_2$	$\vec{E} \perp \vec{c}$	10.7	144	12.5	5.90	204	3.71
	$\vec{E} \| \vec{c}$	9.42	241	0.60	9.16	248	1.36

		ρ_{opt} (Ω cm)	ρ_{dc} (Ω cm)	N (cm^{-3})	μ (cm^{2}V^{-1}sec^{-1})
		Plasmons		dc measurements	
SnS_2	$\vec{E} \perp \vec{c}$	1.11	0.60	2×10^{17}	51.5
$SnSe_2$	$\vec{E} \perp \vec{c}$	0.28	0.27	7.9×10^{17}	29.3

where $\bar{m}$ is the mode mass and N_0 is the oscillator density. For the CdI_2 structure, $\bar{m} = m_{Sn}m_X/(m_{Sn} + 2m_X)$, where we have written SnX_2. A second property of interest is the LO phonon frequency. This is obtained from a determination of the position of the peak in $-Im[1/\epsilon(\nu)]$ (see Fig. 2). For this calculation we include only the phonon contribution. For the $\vec{E} \perp \vec{c}$ polarization, including the overdamped plasmons produces a small shift of the coupled and broadened LO modes to higher frequency, ~ 4 cm^{-1} in SnS_2 and 9 cm^{-1} in $SnSe_2$.

Before discussing the important anisotropies in the phonon properties, we note the agreement between the dc resistivity and the resistivity as calculated from the oscillator fit parameters. Since the plasmons are overdamped we can only determine a resistivity and not the values for N/m^* and τ separately. The dc and optical resistivities are also included in Table I.

FORCE-CONSTANT MODEL

In order to understand the anisotropy in the phonon frequencies in a quantitative way we must also consider the frequencies of the Raman active modes. These have been determined[9] and are included in Table II. The anisotropies to be explained are (i) the difference in the two Raman frequencies, $\nu(A_{1g}) - \nu(E_g) = 107$ cm^{-1} for SnS_2 and 73 cm^{-1} for $SnSe_2$; (ii) the difference in the two TO phonon modes, $\nu(A_{2u}) - \nu(E_u) = 135$ cm^{-1} for SnS_2 and 97 cm^{-1} for $SnSe_2$, and finally, (iii) the difference in the reststrahl bandwidths for the two polarizations, $[\nu_{LO}(E_u) - \nu_{TO}(E_u)] - [\nu_{LO}(A_{2u}) - \nu_{TO}(A_{2u})] = 93$ cm^{-1} for SnS_2 and 53 cm^{-1} for $SnSe_2$.

Simplified force-constant models have been applied to the layered crystals to identify the large differences between the intralayer and interlayer forces.[8] The approach taken in this paper is more generalized, treating the intralayer and Coulomb forces in greater detail. We use a valence-force-field (VFF) formulation[14] to describe the harmonic restoring forces and then consider the Coulomb

contributions. In the VFF model, the harmonic forces result from an (r, θ) representation of the energy, where r is a bond length and θ a bond angle. For layer crystals we consider two types of bonds, bonds within the layers denoted by r and bonds between the layers by R, a similar notation is used for the bond angles, θ and Θ. In the VFF model, the energy is expanded to second order in the deviations from the equilibrium bond lengths and bond angles, Δr and $\Delta \theta$, and ΔR and $\Delta \Theta$. We neglect terms in $\Delta \Theta$, assuming these to be smaller than the other terms we retain. The harmonic energy U is then given by

$$U = \sum \left[\tfrac{1}{2}k_r(\Delta r)^2 + \tfrac{1}{2}k_R(\Delta R)^2\right]$$
$$+ \sum{}' \left[\tfrac{1}{2}k_\theta(r_0\Delta\theta)^2 + k_{rr'}\Delta r\Delta r' + k_{r\theta}\Delta r(\Delta\theta)r_0\right], \quad (9)$$

where the k's are the VFF forces and r_0 is an equilibrium bond length. The energy is separated into two sums.[15] The k_r and k_R terms depend only on distances between two atoms (two-body forces) and hence are the central forces present in all bonding mechanisms. The sum is then over all pairs of relevant atoms. The remaining terms depend on the positions of three atoms (three-body forces) and are the noncentral forces important in covalent bonding, e.g., bond-bending forces. We have neglected terms that represent interactions between intralayer and interlayer bonds, e.g., $k_{rR}\Delta_r\Delta_R$. However, these forces as well as terms in k_Θ, must be included in fitting the full dispersion curves.[15, 16]

Expressions for the zone-center modes, $\Gamma = A_{1g} + A_{2u} + E_g + E_u$, have been developed by considering the idealized CdI_2 structure. These calculations are discussed in detail in another publication.[16] We first note that the c/a ratio for idealized CdI_2 is 1.63 so that the ratios for SnS_2 and $SnSe_2$, 1.613 and 1.61, respectively, are very nearly ideal. The following expressions result:

TABLE II. Zone-center optic modes.

| Material | Raman modes (cm^{-1}) | | ir modes (cm^{-1}) | | | |
	$\nu(A_{1g})$	$\nu(E_g)$	$\nu_{TO}(A_{2u})$	$\nu_{LO}(A_{2u})$	$\nu_{TO}(E_u)$	$\nu_{LO}(E_u)$
SnS_2	315	208	340	356	205	314
$SnSe_2$	186	113	241	248	144	204

Phonon anisotropies (cm^{-1})	$\nu(A_{1g}) - \nu(E_g)$	$\nu_{TO}(A_{2u}) - \nu_{TO}(E_g)$	$[\nu_{LO}(E_u) - \nu_{TO}(E_u)]$ $-[\nu_{LO}(A_{2u}) - \nu_{TO}(A_{2u})]$
SnS_2	107	135	93
$SnSe_2$	73	97	53

$$m_x \nu^2(A_{1g}) = k_r + k_{rr'} + 8k_\theta + 3.6k_R ,$$

$$m_x \nu^2(E_g) = k_r + k_{rr'} + 2k_\theta + 1.2k_R ,$$ (10)

$$\bar{m}\nu^2(A_{2u}) \equiv \bar{m}\nu^2(E_u) = k_r - k_{rr'} + 4k_\theta - 8k_{r\theta} .$$

This calculation predicts the observed anisotropy in the Raman modes $\nu(A_{1g}) > \nu(E_g)$, but fails to account for the observed splitting of the ir modes $\nu(A_{2u}) > \nu(E_u)$. The disparity between the VFF model and experiment for the ir modes is removed when we consider the contributions due to Coulomb forces. The effect of such forces on the TO phonon frequencies is model dependent.[17-19] In semiconductors, it is appropriate to separate the macroscopic charge as e_T^* into a local part, e_l^* and a nonlocal part. This separation of e_T^* leads to the following expressions for the TO and LO phonon frequencies[20, 21]:

$$\nu_{TO}^2(j) = \nu_0^2 - 4\pi L_j(N_0/\bar{m})[e_l^*(j)]^2 ,$$

$$\nu_{LO}^2(j) = \nu_{TO}^2(j) + 4(N_0/\bar{m})[e_T^*(j)]^2/\epsilon_\infty(j) ,$$ (11)

where j indicates the polarization and where ν_0 is the mechanical or "spring-constant" frequency; e.g., the frequency calculated in the VFF model. From Ref. 22, we obtain the expressions for L_j, for $c/a > 1$,

$$L_x = L_y = 0.37(c/a) , \quad L_z = 1 - 0.74(c/a) .$$ (12)

The charges defined in (11) for the CdI_2 lattice are those on the Sn atom. For $c/a \approx 1.61$, $L_x, L_y = 0.60$ and $L_z = -0.20$. Therefore, the inclusion of dipolar coupling serves to increase the frequency $\nu_{TO}(A_{2u})$ with respect to ν_0, but to decrease the frequency $\nu_{TO}(E_u)$. Thus, the inclusion of these Coulomb contributions removes the degeneracy in these modes that arises in the VFF model. Before we treat this quantitatively, let us consider

the Coulomb contributions to the Raman modes.

These contributions are approximated by noting that charge neutrality within the unit cell requires charges of $\frac{1}{2}|e_l^*(j)|$ on the chalcogenide atoms. The Raman modes involve out of phase displacements of the chalcogenide atoms with the Sn atoms at rest.[7] The chalcogenide atoms occupy sites on an approximately fcc lattice and the resultant Raman modes are equivalent to zone-boundary modes of this lattice. Dipole sums have been computed for these lattices[23] so that it is a simple matter to write the appropriate Coulomb terms; these are given by

$$m_x \Delta\nu^2(A_{1g}) = 1.80N_0[e_l^*(\|)]^2 ,$$

$$m_x \Delta\nu^2(E_g) = -0.90N_0[e_l^*(\perp)]^2 .$$ (13)

These dipolar contributions add to the anisotropies already evident in the force-constant model [see Eq. (8)]. Combining Eqs. (10), (11), and (13), and for simplicity, assuming $e_l^*(\|) = e_l^*(\perp) = e_l^*$, we obtain the following expressions for the zone-center modes:

$$m_x \nu^2(A_{1g}) = k_r + k_{rr'} + 8k_\theta + 3.6k_R + 1.80N_0(e_l^*)^2 ,$$

$$m_x \nu^2(E_g) = k_r + k_{rr'} + 2k_\theta + 1.2k_R - 0.90N_0(e_l^*)^2 ,$$

$$\bar{m}\nu_{TO}^2(A_{2u}) = k_r - k_{rr'} + 4k_\theta - 8k_{r\theta} + 2.41N_0(e_l^*)^2 ,$$

$$\bar{m}\nu_{LO}^2(A_{2u}) = m\nu_{TO}^2(A_{2u}) + [4\pi N_0/\epsilon_\infty(\|)][e_T^*(\|)]^2 ,$$ (14)

$$\bar{m}\nu_{TO}^2(E_u) = k_r - k_{rr'} + 4k_\theta - 8k_{r\theta} - 7.49N_0(e_l^*)^2 ,$$

$$\bar{m}\nu_{LO}^2(E_u) = \bar{m}\nu_{TO}^2(E_u) + [4\pi N_0/\epsilon_\infty(\perp)][e_T^*(\perp)]^2 .$$

Also included in Eqs. (14) are expressions for the LO modes. These incorporate the definitions for $e_T^*(j)$.
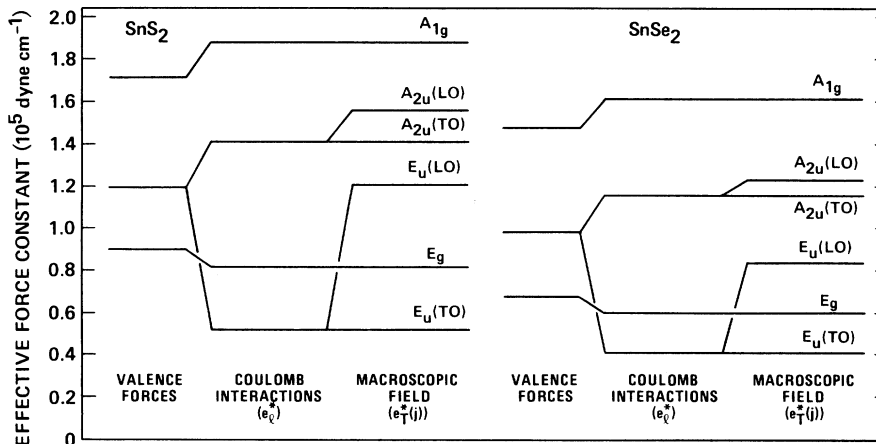
FIG. 3. Schematic representation of the forces contributing to the optic-mode frequencies of SnS_2 and $SnSe_2$ [see Eqs. (10), (11), (13) and (14)] .

APPLICATION TO SnS$_2$ AND SnSe$_2$

The procedure used to quantify the phonon anisotropies is illustrated in Fig. 3. We start with the experimentally determined frequencies, multiplied by the appropriate mass $m_j \nu_j^2$ [see Eq. (14)]. If the ν_j are in cm^{-1} and the m_j are in atomic mass units, then multiplication of these terms by 0.059 gives the k_m in dyn cm^{-1}.

Consider first the LO-TO splittings of the ir-active modes. These splittings define the $e_T^*(j)$. $e_T^*(\perp) > e_T^*(\parallel)$ by approximately a factor of 3 for both SnS$_2$ and SnSe$_2$. Similar differences, but smaller in magnitude, have been found for PbI$_2$ and CdI$_2$.[5] The effective charges in SnS$_2$ and SnSe$_2$ as well as those in PbI$_2$ contain large dynamic contributions.[5,6] In principal, these can be deduced from the band structure and we are currently pursuing this calculation.

The difference in frequency between the TO modes for $\vec{E} \parallel \vec{c}$ and $\vec{E} \perp \vec{c}$ is used to define a local effective charge e_I^*. We obtain similar values of e_I^* for SnS$_2$ and SnSe$_2$, $1.63e$ and $1.59e$, respectively. Since the charge on the Sn atom for a completely ionic bond is $4e$, we can define a bond ionicity by comparing e_I^* with $4e$. This leads to ionicities of ~0.4 for SnS$_2$ and SnSe$_2$. Similar calculations for PbI$_2$ and CdI$_2$ yield $e_I^* \sim 1.2e$ and hence ionicities of ~0.6.[6] These relative ionicities are anticipated on the basis of other properties, e.g., the optical-frequency dielectric constants[24] and the anion-radius–cation-radius ratios,[25] as well as the electronegativity differences of the appropriate pairs of atoms.[26]

Having obtained e_I^* we can then find the contribution to the TO modes from the VFF forces. This is also illustrated in Fig. 3. We can also calculate the Coulomb contributions to the Raman modes and thereby allow a comparison with the VFF model for these modes as well. Consider first the reduced Raman frequencies. The differences between the A_{1g} and E_g frequencies are due to two types of forces, intralayer noncentral or three-body interactions and interlayer forces. Similarly the difference in frequency between either one of the Raman modes and the VFF ir mode is also due to the same types of forces [see Eq. (10)]. Since we have introduced more VFF forces than we have

frequencies, we would have to make arbitrary assumptions about some of the k_m to generate a set of forces. We note here that such an analysis is only possible if the full dispersion curves have been obtained. For SnS$_2$ and SnSe$_2$, the reduced frequencies, those obtained after removal of the Coulomb terms, are consistent with values of k_r being greater than k_R and the noncentral intralayer forces, k_θ, $k_{rr'}$, and $k_{r\theta}$.

SUMMARY AND CONCLUSIONS

The most important aspect of this study is the explanation of the frequency differences for the in-plane and out-of-plane Raman and ir modes. Consider first the ir-active modes. The large difference in frequency between $\nu_{TO}(A_{2u})$ and $\nu_{TO}(E_u)$ is the result of Coulomb contribution to the local field. The difference in these two frequencies for CdI$_2$-structured crystals then provides a direct measure of a local effective charge,[20,21] in our formulation a charge on the Sn atoms. Comparison of this charge with $4e$ then yields an estimate of the ionic contribution to the bonding. The differences in the reststrahl bandwidths $\nu_{LO}(j)$ $- \nu_{TO}(j)$ for the two polarizations gives significant differences in the macroscopic effective charges, for SnS$_2$ and SnSe$_2$, $e_T^*(\perp)/e_T^*(\parallel) \approx 3$. This is direct evidence for large dynamic contributions to both $e_T^*(j)$. Finally, the differences in the two Raman frequencies result from three different effects, noncentral intralayer forces, interlayer forces, and relatively small Coulomb contributions. A more complete parametrization of the VFF forces can only be accomplished when phonon-dispersion curves become available.

Note added in proof. The lattice dynamics of CdI$_2$-structured crystals have also been studied using central-force (CF) models. The differences between VFF and CF models are discussed in another publication[27] where we show that CF models are adequate for more ionic crystals, e.g., PbI$_2$, but not for SnS$_2$ and SnSe$_2$. Secondly, an estimate of the ionicity of a crystal must take into account the atomic coordination and availability of bonding electrons as well as the electronegativity difference.[26] This point is also addressed in Ref. 27.

[1] J. L. Verble and T. J. Wieting, Phys. Rev. Lett. 25, 362 (1970); T. J. Wieting and J. L. Verble, Phys. Rev. B 3, 4286 (1971); and J. L. Verble, T. J. Wieting and P. R. Reed, Solid State Commun. 11, 941 (1972).

[2] P. C. Leung, G. Andersman, W. G. Spitzer, and C. A. Mead, J. Phys. Chem. Solids 27, 849 (1966); T. J. Wieting and J. L. Verble, Phys. Rev. B 5, 1473 (1972);

J. C. Irwin, R. M. Hoff, B. P. Clayman, and R. A. Bromley, Solid State Commun. 13, 1531 (1973); M. Hayek, O. Brafman and R. M. A. Lieth, Phys. Rev. B 8, 2772 (1973); A. Mercier and J. P. Voitchovsky, Solid State Commun. 14, 757 (1974); E. Finkman and A. Rizzo *ibid*. 15, 1841 (1974).

[3] R. Zallen, M. L. Slade and A. T. Ward, Phys. Rev.

B 3, 4257 (1971).

[4]D. Treacy and P. C. Taylor, Phys. Rev. B 11, 2941 (1975).

[5]R. Zallen and M. L. Slade, Solid State Commun. 17, 1561 (1975); and G. Lucovsky, R. M. White, W. Y. Liang, R. Zallen, and Ph. Schmid, ibid. 18, 811 (1976).

[6]J. C. Mikkelsen, Jr., G. Lucovsky, R. M. Martin, R. Zallen, and M. L. Slade, Bull. Am. Phys. Soc. 21, 225 (1976).

[7]J. E. Smith, Jr., M. I. Nathan, M. W. Shafer, and J. B. Torrance, in Proceedings of the Eleventh International Conference on the Physics of Semiconductors (Polish Scientific, Warsaw, 1972), p. 1306; and G. Lucovsky, R. M. White, J. A. Benda, and J. F. Revelli, Phys. Rev. B 7, 3859 (1973); and G. Lucovsky, W. Y. Liang, R. M. White, and K. R. Pisharody, Solid State Commun. (to be published).

[8]R. Zallen and M. L. Slade, Phys. Rev. B 9, 1627 (1974); and R. Zallen, Proceedings of the Twelfth International Conference on the Physics of Semiconductors (Teubner, Stuttgart, 1974), p. 621.

[9]A. J. Smith and W. Y. Liang (private communication).

[10]A. S. Barker, Jr., Phys. Rev. 165, 917 (1968).

[11]B. B. Varga, Phys. Rev. 137, A1896 (1965); and E. Burstein, in Dynamical Processes in Solid State Optics (Benjamin, New York, 1967).

[12]D. T. Hon and W. L. Faust, J. Appl. Phys. 1, 241 (1973).

[13]E. Burstein, M. H. Brodsky and G. Lucovsky, J. Quantum Chem. 1S, 759 (1967).

[14]M. J. P. Musgrave and J. A. Pople, Proc. R. Soc. 260, 474 (1962).

[15]R. M. Martin, G. Lucovsky and K. Helliwell, Phys. Rev. B 13, 1383 (1976).

[16]R. Zallen, G. Lucovsky and R. M. Martin (unpublished).

[17]B. Szigeti, Trans. Faraday Soc. 45, 155 (1949).

[18]J. Tessman, A. Kahn, and W. Shockley, Phys. Rev. 92, 890 (1953).

[19]M. H. Brodsky and E. Burstein, J. Phys. Chem. Solids 28, 1655 (1967).

[20]F. Stern, Elementary Theory of the Optical Properties of Solids, Solid State Physics, edited by F. Seitz and D. Turnbull (Academic, New York, 1964), Vol. 15.

[21]G. Lucovsky, R. M. Martin, and E. Burstein, Phys. Rev. B 4, 1367 (1971).

[22]H. Mueller, Phys. Rev. 50, 547 (1936).

[23]E. W. Kellermann, Philos. Trans. R. Soc. 238, 513 (1940); Proc. R. Soc. A 178, 17 (1941).

[24]J. C. Phillips and J. A. VanVechten, Phys. Rev. Lett. 22, 705 (1969).

[25]R. M. White and G. Lucovsky, Solid State Commun. 11, 1369 (1972).

[26]L. Pauling, The Nature of the Chemical Bond (Cornell U.P., Ithaca, N.Y., 1960).

[27]G. Lucovsky and R. M. White, in Proceedings of the Conference on Layered Semiconductors and Metals, 1976, Bari, Italy (unpublished).